

# ANALYSIS OF RECENT CZ-6A ROCKET UPPER STAGE FRAGMENTATIONS

Daniel R. Wacker<sup>(1)</sup>, Teresa Klinner-Teo<sup>(1)</sup>, Jennifer Ly<sup>(1)</sup>, Carsten Wiedemann<sup>(1)</sup>, Manuel Metz<sup>(2)</sup>,  
Simona Silvestri<sup>(1)</sup>

<sup>(1)</sup>*Institute of Space Systems, Technische Universität Braunschweig, 38108 Braunschweig, Germany,  
Email: {d.wacker, teresa.klinner-teo, j.ly, c.wiedemann, simona.silvestri}@tu-braunschweig.de*

<sup>(2)</sup>*Deutsche Raumfahrtagentur im DLR, German Aerospace Center, 53227 Bonn, Germany,  
Email: manuel.metz@dlr.de*

## ABSTRACT

Orbital fragmentation events are the largest source of space debris objects bigger than 10 cm in the near-Earth environment, resulting in the need for regular, cost-intensive collision avoidance maneuvers. The most significant increase in long-term collision risk in the recent years stems from the breakups of the CZ-6A upper stages 2022-151B and 2024-140U on sun-synchronous orbits, resulting in over 650 cataloged fragments each. This paper presents an investigation into these fragmentations, compares them with each other and illustrates the effects they have on the space environment. The performed simulations utilize TLE data, fragmentation models and propagators to determine the exact time and location of the fragmentation events, the resulting additional velocity vector distributions of the cataloged fragments as well as the predicted remaining fragments' orbital lifetimes. Furthermore, the increase in spatial density resulting from both events and the collision risk for objects in their proximity are computed.

Keywords: Fragmentation; breakup; CZ-6A upper stage; analysis; modeling; simulation; orbital lifetime; additional velocity vector; spatial density; collision risk.

## 1 INTRODUCTION

Since the beginning of spaceflight, on average about 10 non-deliberate fragmentation events of human-made objects in Earth orbit have occurred every year [1]. The severity and relevance of these events, however, vary as all types of catastrophic and non-catastrophic breakups are accounted for. Although the number of released fragments per breakup changes significantly for that reason, it can be calculated that for the events for which fragments could be cataloged, on average approximately 48 fragments per event are recorded on Spacetrack [2], [3]. This high average number of historic fragmentations per year and fragments per event has led to a continuously increasing number of cataloged fragments remaining in orbit, despite the decay of many fragments over time due to the atmospheric drag. Moreover, only fragments larger than about 10 cm can be reliably tracked and cataloged but orders of magnitude

more smaller untrackable fragments are generated that also pose a critical collision risk [3]. Due to the high kinetic energy involved in orbital collisions with relative velocities of up to 15 km/s, an impacting fragment with a size of 1 cm to 10 cm can be mission ending for active spacecraft or even lead to a partial or complete fragmentation of all types of larger space objects.

Therefore, it is important to model and analyze fragmentation events as well as their relevant characteristics to understand and estimate the temporal and spatial evolution of the risk they pose to the space environment. The modeling and analysis of fragmentation events began in the 1970s with the NASA (National Aeronautics and Space Administration) Orbital Debris Office Program and has since resulted in various models and analysis tools, such as the NASA SBM (Standard Breakup Model), Battelle model, FASTT (Fragmentation Algorithms for Strategic and Theater Targets) model, IMPACT model, FREMAT (FRAGMENTATION Event Model and Assessment Tool), CST (Collision Simulation Tool), PUZZLE tool and CARDC-SBM (China Aerodynamics Research and Development Center-Spacecraft Breakup Model) [4-11].

The analyses conducted in this paper are based on data processing performed with the MASTER tool-chain, which uses an adapted version of the NASA SBM, as well as an in-house developed tool named ORFANT (ORbit Fragmentation ANalysis Tool) [12], [13].

This paper focuses on the fragmentation of the CZ-6A (Chang Zheng 6A) upper stages with the COSPAR IDs (Committee on Space Research International Designators) 2022-151B and 2024-140U, which are of particular interest as they generated over 650 cataloged fragments each and occurred in an orbital region with a high spatial density as well as a long orbital lifetime for fragments. Therefore, this paper aims to investigate important characteristics of these events and to assess their long-term impact on the space environment. After a short summary of the current insights into the events, the simulation results for the fragmentation location and epoch, additional velocity vectors, fragments' orbital lifetime, spatial density and collision risk are illustrated.

## 2 CURRENT INSIGHTS

On 12 November 2022, the CZ-6A upper stage 2022-151B with a dry mass of 5800 kg suffered a major breakup in a sun-synchronous orbit with a perigee height of 813 km, an apogee height of 847 km and an inclination of  $98.8^\circ$  [14]. At the time of writing, 793 fragments from this event have been cataloged on Spacetrack [3]. Initial analyses of the event, highlighting e.g. the Gabbard diagram, estimated fragmentation epoch and spreading velocities of the fragments, have been conducted in [14-16] using TLE (Two Line Elements) data, the IMPACT model and the PUZZLE software. It is assumed that the breakup was caused by an unintentional explosion [14].

The second and third known fragmentation of a CZ-6A upper stage occurred for the upper stages 2024-058B and 2024-126D on 02 April 2024 and 05 May 2024 respectively, according to DISCOS (Database and Information System Characterising Objects in Space) [2]. However, at the time of writing, no fragments were cataloged on Spacetrack for these fragmentations, and since the analyses performed in this paper are based on TLE data, these events are not further investigated [3].

On 06 August 2024, the last and most recent CZ-6A fragmentation occurred for the upper stage 2024-140U in a sun-synchronous orbit with a perigee height of 797 km, an apogee height of 857 km and an inclination of  $89^\circ$  [17]. So far, 664 fragments have been cataloged for this event on Spacetrack and there is no known scientific publication about this fragmentation aside from the above cited one [3].

## 3 ORBIT FRAGMENTATION ANALYSIS TOOL (ORFANT)

The in-house developed tool ORFANT is used to conduct different analyses for this study. This chapter provides a brief introduction to the tool. ORFANT can be used to determine the breakup epoch, the location within the parent's orbit where the fragmentation occurred and the fragments' additional velocity vectors based on TLE data of the parent and the fragments. The processing within the tool can be divided into the following six main tasks:

1. Automated TLE data download
2. Identification of fragments from the event
3. Backpropagation to initially estimated epoch
4. Determination of breakup epoch
5. Determination of breakup location within orbit
6. Determination of additional velocity vectors

First, the TLE data of the parent and all debris objects from the launch that correspond to the parent object's COSPAR ID core are downloaded from Spacetrack. Automated and manual filters are then applied to identify

all debris objects from the launch that belong to the event. This is particularly relevant for fragmentation events of objects from a launch for which multiple breakups occurred. Next, all objects that belong to the event are backpropagated to different points in time close to an initial epoch estimate based on DISCOS. Afterwards, different distance metrics, which are further discussed in Chapter 4 and 5, can be used to estimate the exact breakup epoch. Furthermore, the location of the fragmentation within the orbit of the parent object can be determined for the estimated epoch. Finally, the additional velocity vectors of all cataloged fragments that belong to the event can be computed for the estimated fragmentation epoch and location. This is of high relevance as the additional velocity vector distribution does not only provide information about the severity and possible causes of the fragmentation but can also be used to improve fragmentation modeling as well as synthetic population generation processes.

## 4 BREAKUP LOCATION WITHIN ORBIT

The fragmentation location within the parent's orbit is determined by dividing the parent orbit at the estimated fragmentation epoch into a defined number of argument of latitude (argument of perigee + true anomaly) values. For each of these points, the distance between the parent orbit and all backpropagated fragment orbits is calculated. As the imparted energy on each fragment of a breakup can be viewed as a single impulsive maneuver, their orbits are all expected to cross the origin of the fragmentation, the so-called pinch point, at the true breakup epoch. Therefore, the parent orbit's AoL (Argument of Latitude) value at which the average distance between the parent orbit and all fragment orbits is minimal is considered to be the most likely point of fragmentation within the parent orbit.

In Figure 1, this calculated distance in dependence of the CZ-6A upper stage 2022-151B orbit's argument of latitude values is plotted for all fragments individually in blue and averaged over all fragments in yellow for an estimated fragmentation epoch of 12 Nov 2022 05:19 UTC (Universal Time Coordinated). The minimum of the yellow curve marks the most likely point within the parent orbit at which the fragmentation may have occurred. At this minimum, with an average distance of 1.8 km between the orbit of the parent and all fragment orbits, the parent argument of latitude is  $74.5^\circ$ . It is worth noting that many fragments also have a second local minimum close to a parent argument of latitude of  $255^\circ$  which is approximately  $180^\circ$  shifted from the global minimum. These are the fragments that were mainly accelerated orthogonal to the parent's orbital plane and thus cross it again  $180^\circ$  after the point of fragmentation within their new orbit. The low average distance of 1.8 km at the global minimum combined with the converging behavior of the minima of the distance plots for the individual fragments increase the confidence in

the determined fragmentation location. Moreover, the resulting average distance could become even lower if more sophisticated propagators than the currently implemented SGP4 (Simplified General Perturbations 4) method are used for the backpropagation of the fragments [18]. This is because some fragments are cataloged only months or even years after the fragmentation event and thus have to be backpropagated for longer periods of time, increasing potential propagation errors. Therefore, only 714 out of the 793 cataloged fragments from 2022-151B are considered for the analyses in this paper. Nevertheless, the accuracy of the used TLE data themselves cannot be influenced, which limits the hypothetically achievable accuracy for their processing.

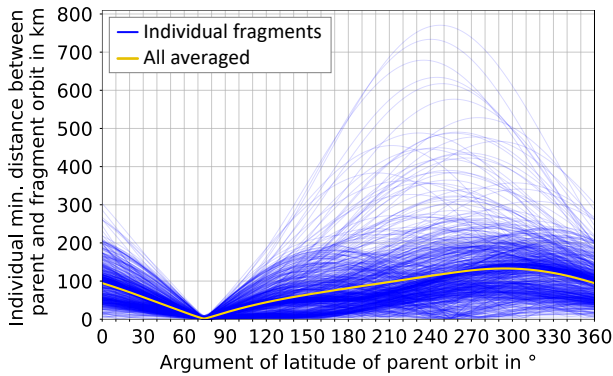


Figure 1. Distance between the orbit of the CZ-6A upper stage 2022-151B and all fragment orbits in dependence of the parent orbit AoL for all fragments individually in blue and all fragments averaged in yellow for an estimated breakup epoch of 12 Nov 2022 05:19 UTC.

Additionally, the influence of potential epoch errors has to be considered with regard to the confidence in the determined fragmentation location. Therefore, in Figure 2, the determined CZ-6A upper stage 2022-151B fragmentation argument of latitude as well as the corresponding minimal average distance between the parent orbit and all fragment orbits at this location are plotted for epochs up to one week around the estimated fragmentation epoch from Figure 1. This illustrates that an epoch error of  $\pm$  one day has only a minor influence of about  $\pm 1.5^\circ$  regarding the determined fragmentation location within the parent orbit in this case. Additionally, the temporal evolution of the minimal average distance between the parent orbit and all fragment orbits shows a clear 'v'-shape with the minimum at the estimated fragmentation epoch 12 Nov 2022 05:19 UTC. This increases the confidence in the estimated fragmentation epoch as well as the determined fragmentation location within the parent's orbital plane.

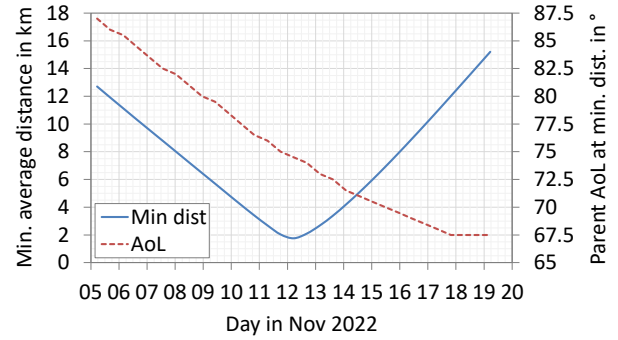


Figure 2. Determined CZ-6A upper stage 2022-151B fragmentation location in red as well as the corresponding minimal average distance in blue between the parent orbit and all fragment orbits for epochs up to one week around the estimated fragmentation epoch 12 Nov 2022 05:19 UTC.

In Figure 3 and 4, the same characteristics as in Figure 1 and 2, are visualized for the CZ-6A upper stage 2024-140U fragmentation with an estimated breakup epoch of 06 Aug 2024 16:52 UTC. Regarding the distance between the parent orbit and all fragment orbits, again a clear convergence to a global minimum is evident for the estimated fragmentation epoch, as illustrated in Figure 3. In this case, the most likely fragmentation point within the parent orbit is at an argument of latitude of  $229.5^\circ$ . For reference, the entire set of Keplerian elements from the orbits of both CZ-6A upper stage events at their determined fragmentation location is given in Table 1.

Table 1. Keplerian elements from the orbits of the CZ-6A upper stages 2022-151B and 2024-140U at their determined fragmentation locations.

Event	2022-151B	2024-140U
Semi-major axis	7208.15 km	7204.67 km
Eccentricity	0.002327	0.004017
Inclination	$98.81^\circ$	$89.02^\circ$
Right ascension of the ascending node	$321.15^\circ$	$350.21^\circ$
Argument of perigee	$346.98^\circ$	$206.16^\circ$
True anomaly	$87.52^\circ$	$23.34^\circ$

The average distance between the 2024-140U parent orbit and all fragment orbits is about 1.9 km at the above-mentioned breakup location. This average distance is similar to the one from 2022-151B, which is again very low compared to the occurring average distances of more than 150 km at other angular positions within the parent orbit. Furthermore, by comparing Figure 1 and 3, it can be observed that for 2024-140U, fewer fragments have a second local minimum shifted by  $180^\circ$  regarding the parent argument of latitude, which means fewer fragments achieved an additional velocity vector that points orthogonal to the parent's orbital plane.

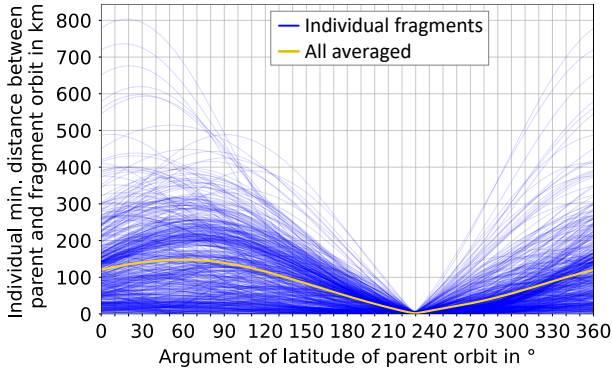


Figure 3. Distance between the orbit of the CZ-6A upper stage 2024-140U and all fragment orbits in dependence of the parent orbit AoL for all fragments individually in blue and all fragments averaged in yellow for an estimated breakup epoch of 06 Aug 2024 16:52 UTC.

Regarding the influence of a varying epoch for the calculation of the fragmentation location within the parent's orbit, Figure 4 displays that the event 2024-140U seems to be slightly more sensitive to earlier epochs. One day earlier would lead to a  $2.25^\circ$  higher parent argument of latitude, while one day later would result in a value about  $0.75^\circ$  lower. Nevertheless, again the average distance between the parent orbit and all fragment orbits at the determined breakup location in dependence of the considered fragmentation epoch shows a clear 'v'-shape with a minimum at the estimated fragmentation epoch 06 Aug 2024 16:52 UTC, increasing the confidence in the determined breakup location and estimated epoch.

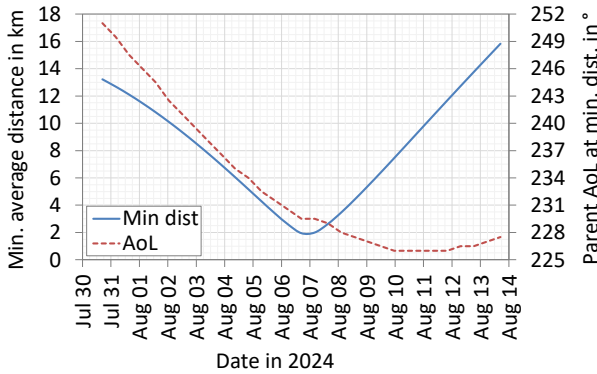


Figure 4. Determined CZ-6A upper stage 2024-140U fragmentation location in red as well as the corresponding minimal average distance in blue between the parent orbit and all fragment orbits for epochs up to one week around the estimated fragmentation epoch 06 Aug 2024 16:52 UTC.

## 5 FRAGMENTATION EPOCH

While the methods used for Figure 2 and 4 can estimate the fragmentation epoch, this section highlights an alternative approach that provides a better converging metric for determining the breakup time. Specifically, it examines the temporal evolution of the average of the

distances between the positions of all possible fragment pairs. All fragments are backpropagated to a set of defined epochs with short time steps (e.g. 1 min) in between. Subsequently, the geometric distance between their actual positions in the Earth-centered inertial frame for all combinations of fragment pairs is calculated and averaged over all pairs. Figure 5 depicts the temporal evolution of this metric for the fragments of the CZ-6A upper stage 2022-151B fragmentation. It shows a clear and strongly converging global minimum of 4751 km at 12 Nov 2022 05:19 UTC. Although this average distance is large compared to the values from Figure 2, the minimum is more pronounced. This arises from the fact that the average pairwise distance between all fragments is very sensitive to the epoch. The initial fragment cloud quickly spreads out regarding the relative angular position of the fragments within their orbit due to varying orbital periods resulting from differences in the additional velocity vectors' magnitudes and directions. For epochs far enough away from the fragmentation time, this effect leads to the metric approaching an almost constant average value resulting from the geometry and size of the fragment orbits. Moreover, the large average pairwise distance between all fragments at the global minimum from Figure 5 also results from propagation as well as TLE data inaccuracies.

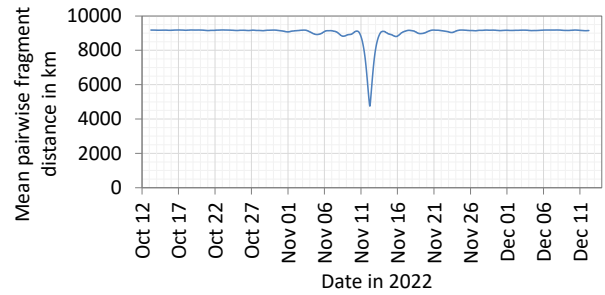


Figure 5. Temporal evolution of the average of the distances between the positions of all possible fragment pairs from the CZ-6A upper stage 2022-151B event.

By considering only fragments that were cataloged a few weeks to months after the event for these calculations, a lower mean pairwise fragment distance can be achieved, as can be seen in Table 2. However, this overview also illustrates that the calculated fragmentation epoch is very stable with regard to the backpropagation time of the CZ-6A 2022-151B fragments as the epoch only varies by about  $\pm 10$  min. Furthermore, the determined fragmentation epochs fit well to the estimated breakup epoch of 12 Nov 2022 05:24-05:29 UTC, given in [14]. As it is desirable to consider as many fragments as possible for the calculations of the additional velocity vector distributions in Chapter 6, the case with a maximum cataloging debut date of 200 days after the event 2022-151B is chosen for the estimation of the fragmentation epoch as well as the breakup location.

Table 2. Overview of calculated CZ-6A 2022-151B fragmentation epochs with a one-minute resolution and mean pairwise fragment distances with different maximal cataloging debut dates of considered fragments.

Max. debut days	Number of considered fragments	Determined fragmentation epoch (UTC, AM)	Mean pairwise fragment distance
12	96	12 Nov 22, 05:37	296 km
30	338	12 Nov 22, 05:28	356 km
55	460	12 Nov 22, 05:23	1047 km
70	503	12 Nov 22, 05:19	1565 km
100	541	12 Nov 22, 05:21	2364 km
200	714	12 Nov 22, 05:19	4751 km

In Figure 6, the temporal evolution of the mean pairwise fragment distance is visualized for the fragments of the CZ-6A upper stage 2024-140U event. Here, a strong convergence to a global minimum can also be identified, which emerges at 06 Aug 2024 16:52 UTC with a mean pairwise fragment distance of 2754 km.

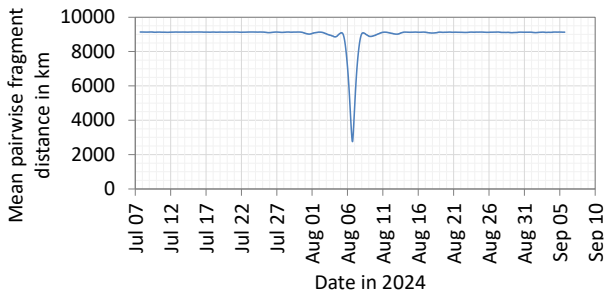


Figure 6. Temporal evolution of the average of the distances between the positions of all possible fragment pairs from the CZ-6A upper stage 2024-140U event.

Comparable to the first CZ-6A upper stage fragmentation, the mean pairwise fragment distance at the global minimum can be reduced by only considering fragments that were cataloged more recently after the 2024-140U event. This is shown in Table 3. Again, the determined fragmentation epoch does not vary significantly, only by  $\pm 17$  min, when the necessary backpropagation time is changed due to different considered maximum cataloging debut dates for the fragments. Additionally, the calculated fragmentation epoch values for 2024-140U fit well to the estimated epoch of 06 Aug 2024 17:15 UTC from [17].

Table 3. Overview of calculated CZ-6A 2024-140U fragmentation epochs with a one-minute resolution and mean pairwise fragment distances with different maximal cataloging debut dates of considered fragments.

Max. debut days	Number of considered fragments	Determined fragmentation epoch (UTC)	Mean pairwise fragment distance
20	92	06 Aug 24, 17:26	389 km
40	263	06 Aug 24, 17:17	916 km
50	365	06 Aug 24, 17:14	1324 km
70	519	06 Aug 24, 16:42	2224 km
100	563	06 Aug 24, 16:52	2754 km

## 6 ADDITIONAL VELOCITY VECTORS

The last step of ORFANT is to calculate the additional velocity vectors of all fragments based on the determined fragmentation epoch and location within the parent orbit. The orbits of all fragments are backpropagated to the estimated fragmentation epoch and then compared with the orbit of the parent directly before the breakup. From changes of the orbital elements of the fragments compared to the pre-fragmentation parent orbit, the gained additional velocity vectors can be calculated if it is assumed that all orbits cross exactly at the determined fragmentation location. Figure 7 illustrates the spatial distribution of the directions of the additional velocity vectors from the fragments of the CZ-6A upper stage 2022-151B event in the parent body centric local horizon reference frame with azimuth  $A$  and elevation  $El$ . The drawn vector  $R$  points in the radial direction extended from Earth's center ( $El = 90^\circ$ ),  $S$  transversal to  $R$  in the direction of movement ( $A = 0^\circ$ ,  $El = 0^\circ$ ) and  $W$  orthogonal to both ( $A = 90^\circ$ ,  $El = 0^\circ$ ), completing the right-handed frame. Two spots of increased density of the fragments' additional vectors can be observed in this reference frame, showing two clear directionalities for their distribution. A significant proportion of the fragments was accelerated into the direction of approximately  $A = -120^\circ$  and  $El = 40^\circ$ , while most other fragments were accelerated in the direction of about  $A = -10$  and  $El = -50^\circ$ . Therefore, the first of the two above-mentioned main fragment clouds has a large additional velocity vector component in the minus  $W$ -direction and thus orthogonal to the orbital plane. For these fragments, mainly the orbital plane rotated, creating a second pinch point on the opposite side of the fragmentation location within the parent orbit. This explains the second local minima of the graphs from the fragments in Figure 1 mentioned in Chapter 4.

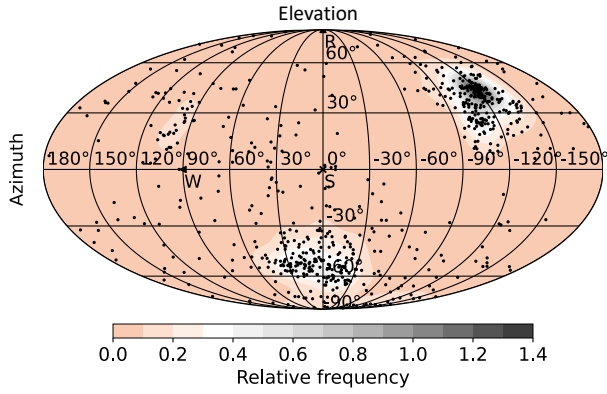


Figure 7. Spatial distribution of the directions of the determined additional velocity vectors of the cataloged fragments from the CZ-6A upper stage 2022-151B event in the parent body centric local horizon reference frame.

For the CZ-6A upper stage 2024-140U fragmentation, the spatial distribution of the additional velocity vectors' directions from the cataloged fragments is visualized in Figure 8. Here, only one region of significantly increased density in the distribution can be observed, which is at an azimuth of about 180° and an elevation of about 40°. However, again the additional velocity vectors show a directionality and not an even omnidirectional distribution as it is assumed in current fragmentation models. Therefore, most of the fragments were decelerated in the direction of movement, leading to a reduction in the semi-major axis of their orbits.

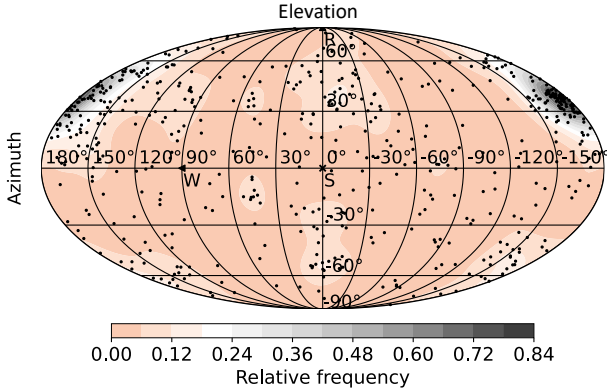


Figure 8. Spatial distribution of the directions of the determined additional velocity vectors of the cataloged fragments from the CZ-6A upper stage 2024-140U event in the parent body centric local horizon reference frame.

In addition to the directionalities of the fragments' additional velocity vectors, their magnitudes are also relevant as they influence by how much the orbital elements are altered due to the fragmentation. Furthermore, it can give indications on the severity of the event. Therefore, in Figure 9, the determined magnitude distribution of the fragments' additional velocity vectors from both CZ-6A upper stage events is plotted. A comparison between both events shows that the additional velocity vector magnitudes for the 2024-140U

event are more spread out and reach higher  $\Delta v$  values, however, the mean value of 64.8 m/s is about 20 % lower than for the 2022-151B event with 80.2 m/s. This indicates that more energy was released in the first CZ-6A upper stage breakup. Based on the differing number of cataloged fragments, no conclusions can be drawn with regard to differences in the total energy released in each breakup as the 2024-140U event occurred so recently that more fragments might be cataloged in the near future.

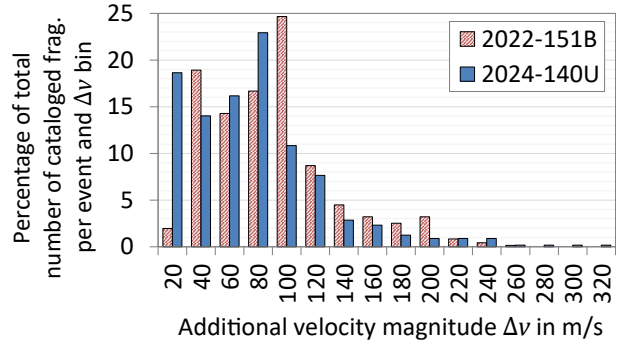


Figure 9. Magnitude distribution of the determined additional velocity vectors of the fragments from both CZ-6A upper stage events.

## 7 FRAGMENTS' ORBITAL LIFETIME

To assess the long-term negative consequences of the CZ-6A upper stage fragmentations on the near-Earth space environment, estimating the orbital lifetime of the fragments is essential. However, for the reasons mentioned in Chapter 1, this is not only the case for the cataloged fragments but also for the fragments larger than about 1 cm that will remain uncataloged due to the limitations of the detection capabilities of the on-ground sensor networks used for the cataloging process. To consider all fragments larger than 1 cm that are expected to have been generated by the events, the CZ-6A upper stage fragmentations were modeled with an adapted version of the NASA SBM used in the MASTER framework, as explained in [12]. Thereby, an explosion is assumed as the breakup cause for both events. Figure 10 shows the simulation results of the temporal evolution of the number of CZ-6A upper stage fragments larger than 1 cm remaining in orbit. Both events are normalized with respect to time by utilizing the number of days after the fragmentation event as the reference. For 2022-151B, more fragments are initially generated within the simulation, as the number of cataloged fragments is used to scale the model. However, both events only lose about 45 % of their initial number of fragments within the simulated three-year period despite the high solar activity and resulting atmospheric, which is currently present and considered in the simulation. The reason for this long lifetime of the fragments is the high perigee altitude of the parent orbits and the low density of the Earth's atmosphere at these altitudes.

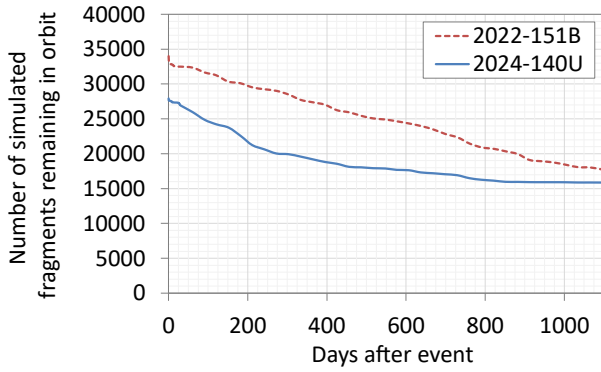


Figure 10. Temporal evolution of the number of simulated CZ-6A upper stage fragments larger than 1 cm remaining in orbit.

Moreover, long-term simulations with future solar activity cycle estimations from CelesTrak [19] were conducted for 10 years after the events. These indicate that over 40% of the fragments larger than 1 cm will remain in orbit during this ten-year period for both events. Therefore, the fragments from each CZ-6A upper stage breakup are expected to have a long-lasting negative effect on the LEO environment, which is further quantified in the following two chapters. This hypothesis is also supported by the current decay behavior of the cataloged fragments from both events, which is visualized in Figure 11. For the 2022-151B fragmentation, only about 15% of the 793 cataloged fragments have re-entered in Earth's atmosphere about 2.35 years after the event, according to data from [3], and the fragments from 2024-140U follow the same trend. These data also indicate that the average cross-sectional area-to-mass ratios of the cataloged CZ-6A upper stage fragments appear to be smaller than expected from fragmentation modeling, since the simulated fragments decay more rapidly. However, further investigations would have to be conducted to confirm that this effect stems from the ballistic coefficient of the fragments and not potential unknown issues of the propagator, including its atmospheric model.

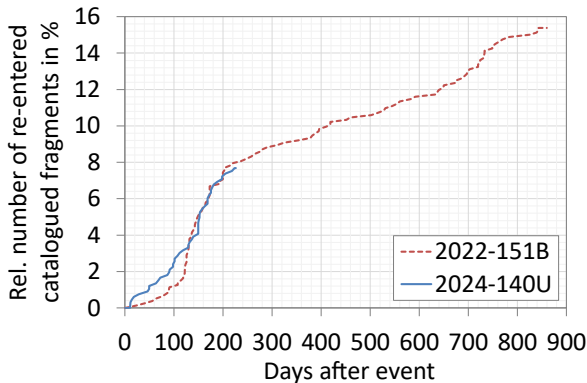


Figure 11. Temporal evolution of the percentage number of re-entered cataloged CZ-6A upper stage fragments by 21 March 2025.

## 8 SPATIAL DENSITY

The spatial density is defined as the number of objects per volume in space, which is needed to calculate expected collision flux values. Therefore, it can be used to assess the impact of fragments from specific breakup events on the space environment. Within the same simulations conducted for the lifetime analyses of the CZ-6A upper stage fragments, the spatial density in dependence of the altitude was computed too. Figure 12 highlights the spatial density in dependence of the altitude for the simulated CZ-6A upper stage 2022-151B fragments at four different epochs and sets it into relation with the background space debris environment based on the condensed MASTER 2016 population for objects larger than 1 cm. As can be seen in Figure 12 a), one month after the event, the simulated 2022-151B fragments result in a large spike for the spatial density, which is more than half as large as the spatial density of the background population at the altitude of the breakup. One year after the event, this peak is reduced and flattened, although it still remains at almost one third of the spatial density of the background population. For three and ten simulated years after the event, the spatial density maximum of the fragments further decreases to about 15% and 10% respectively of the background population's spatial density at an altitude of approximately 800 km, highlighting the long-term significance of this event. Thereby, the background population is purposefully not propagated or updated to future estimations of the population to ensure comparability with the other CZ-6A upper stage fragmentation.

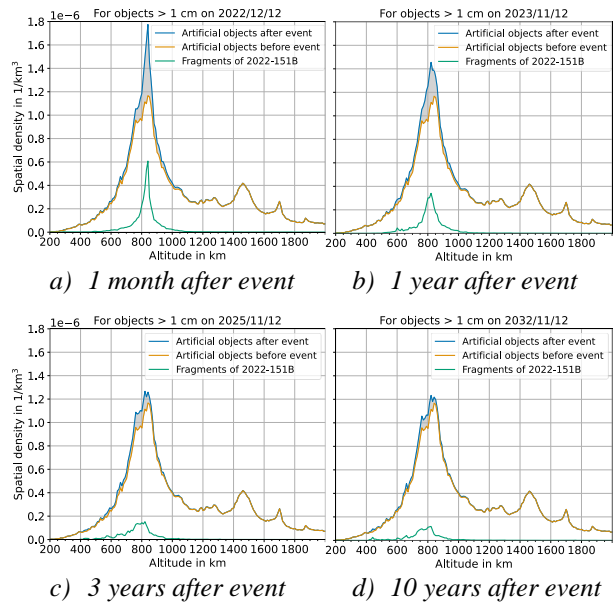


Figure 12. Spatial density of the simulated CZ-6A upper stage 2022-151B fragments in comparison with the condensed MASTER 2016 population in dependence of the altitude for objects larger than 1 cm at different times after the event.

In Figure 13, the same types of spatial density plots as in Figure 12 are presented for the CZ-6A upper stage fragmentation 2024-140U. The initial peaks one month and one year after the 2024-140U event are slightly lower than for 2022-151B, as fewer fragments were cataloged and thus generated in the simulation. Furthermore, the fragmentation of 2024-140U occurred more closely to the peak of the current solar activity cycle, meaning that the fragments are initially decelerated more strongly due to the higher drag force. Three and ten years after the event, the maximum values of the spatial density altitude distribution of the fragments from 2024-140U correspond to about 20% and 10% respectively of the background CZ-6A upper stage fragmentation. This indicates that the second CZ-6A upper stage fragmentation is also expected to have a significant long-term effect on the space environment at altitudes close to 800 km.

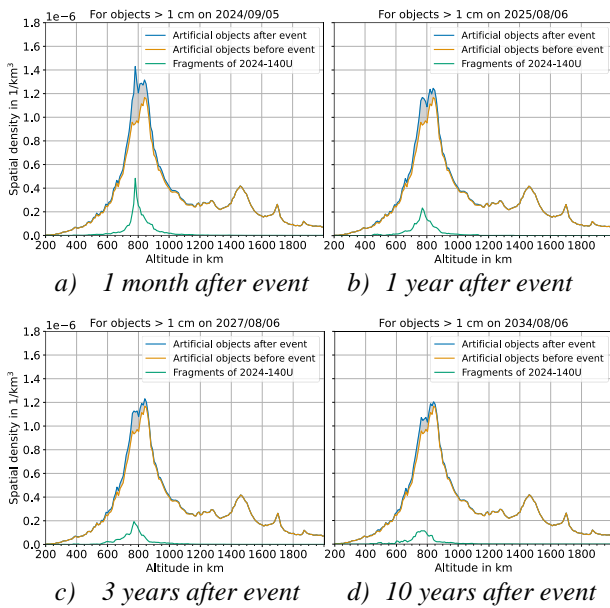


Figure 13. Spatial density of the simulated CZ-6A upper stage 2024-140U fragments in comparison with the condensed MASTER 2016 population in dependence of the altitude for objects larger than 1 cm at different times after the event.

## 9 COLLISION RISK

To further assess the long-term impact of the CZ-6A fragmentations on the space environment, the collision flux was determined within the same simulations conducted for Chapter 7 and 8. Satellites with different mean orbit heights and inclinations were chosen as example target objects, to calculate the expected incoming collision flux on their orbits. The chosen target satellites are highlighted with red circles in Figure 14, which illustrates the inclination and mean height of the orbits of all payloads within the Spacetrack SatCat (Satellite Catalog) as of 27 February 2025 [3].

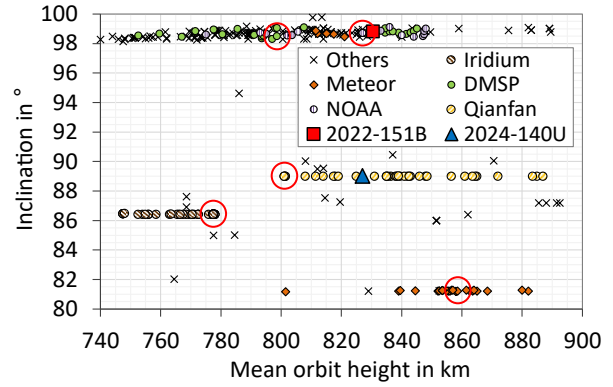


Figure 14. Inclination over mean orbit height (semi-major axis minus 6378 km) of all payloads from the Spacetrack SatCat on 27 February 2025 and both CZ-6A upper stage fragmentation orbits with red circles around selected targets for collision flux analyses.

Furthermore, the corresponding parameters of the breakup orbits of both CZ-6A upper stage events are visualized in this figure with a red square and a blue triangle. Although one of the chosen target satellites stems from the Qianfan group at an inclination of  $i = 89^\circ$ , it shall be noted that these Qianfan satellites are currently in their spiraling-up process until they reach the constellation altitude of 1069 km ( $a = 7447$  km). However, the chosen satellite Qianfan 7 appears to be malfunctional as it is the only one from its launch that does not spiral up in altitude. The results of the collision flux analyses for both simulated CZ-6A upper stage fragments on the chosen targets are shown in Table 4.

Table 4. Overview of the yearly collision flux from the simulated 2022-151B and 2024-140U fragments larger than 1 cm averaged over 10 years after the events on different target satellite orbits in absolute values and relative to the condensed MASTER 2016 population flux.

Target satellite	Absolute flux from 2022-151B in $1/(\text{m}^2\text{yr})$	Absolute flux from 2024-140U in $1/(\text{m}^2\text{yr})$	Relative flux from 2022-151B	Relative flux from 2024-150U
DMSP 4A F2 (1967-010A)	$5.60 \cdot 10^{-5}$	$4.63 \cdot 10^{-5}$	16.57 %	13.71 %
NOAA 20 (2017-073A)	$2.38 \cdot 10^{-5}$	$3.49 \cdot 10^{-5}$	6.10 %	8.90 %
Qianfan-7 (2024-140G)	$4.24 \cdot 10^{-5}$	$1.56 \cdot 10^{-5}$	11.25 %	4.17 %
Iridium 106 (2017-003A)	$5.08 \cdot 10^{-5}$	$6.79 \cdot 10^{-5}$	14.15 %	18.89 %
Meteor 2-7 (1981-043A)	$1.72 \cdot 10^{-5}$	$1.39 \cdot 10^{-5}$	3.51 %	2.83 %

Although the flux varies across the different targets and from event to event, which can be caused by local phenomena of the relative geometry between the target orbit and the fragmentation cloud, the yearly flux from each event averaged over all targets amounts to about

10% of the background flux over the 10 simulated years. These results align well with the long-term spatial density increase discussed in Chapter 8 and further indicate that the CZ-6A upper stages are expected to have significant negative long-term effects on the space environment. A 10% increase in the yearly collision flux averaged over 10 years after the events would also correspond roughly to a 10% increase in the collision probability for this period, and with the fragment clouds from both events to an increase by about 20%. However, these probability values are only derived based on the current number of cataloged fragments and thus might rise in the future when more fragments are detected and cataloged.

## 10 CONCLUSIONS AND OUTLOOK

In this paper, the fragmentations of the CZ-6A upper stages with the COSPAR IDs 2022-151B and 2024-140U were analyzed by simulating and determining different characteristics of the events. The location of the fragmentation within the orbit and the breakup epoch could be determined with methods showing a good robustness against uncertainties for both events. According to the simulations, the fragmentations occurred at a parent AoL of  $74.5^\circ$  and  $229.5^\circ$  on 12 Nov 2022 05:19 UTC and 06 Aug 2024 16:52 UTC, respectively, for the events 2022-151B and 2024-140U. Based on this information, the distribution of the directionality as well as the magnitude of the additional velocity vectors of the cataloged fragments were determined. Differing from expectations of current fragmentation models, the additional velocity vectors show clear directionalities for both events that align well with observed changes from the fragments' orbits. The average magnitude of the fragments' additional velocity vectors from 2022-151B amounts to 80.2 m/s, which is 24% larger compared to 2024-140U, indicating that slightly more energy was released during the first CZ-6A upper stage breakup.

Furthermore, the orbital lifetime analyses show that the effects of the fragments on the space environment are expected to be long-lasting over years or even decades. Moreover, the cataloged fragments are decaying significantly slower than expected from the performed simulations, indicating an even longer lasting negative effect of the fragments. Finally, the spatial density and collision flux analyses show the extent of the temporal and spatial evolution of the negative consequences of both events on the space environment. The ten-year collision risk for many satellites and other space objects in the 800 km altitude orbit regime is expected to have increased by about 20% due to the fragments released from the CZ-6A upper stages. This will result in numerous additionally required collision avoidance maneuvers for active satellites and increases the risk for collisions with all space objects in the mentioned orbit regime that cannot be maneuvered. The shown analysis methods can be used to investigate and characterize

future fragmentation events as well as revisit historic events to potentially gain further insights into the space debris environment and improve the underlying models used for population generation processes and long-term stability simulations.

## ACKNOWLEDGMENT

The research leading to this publication was funded by the German Federal Ministry for Economic Affairs and Climate Action (Bundesministerium für Wirtschaft und Klimaschutz) within the framework of the research project 'A systematic study of the formation processes of space debris objects' under the funding code 50LZ2309.

## REFERENCES

1. ESA (European Space Agency): 'ESA's Annual Space Environment Report', [https://www.esa.int/Space\\_Safety/Space\\_Debris/ESA\\_Space\\_Environment\\_Report\\_2024](https://www.esa.int/Space_Safety/Space_Debris/ESA_Space_Environment_Report_2024), 2024
2. ESA: 'DISCOSweb (Database and Information System Characterising Objects in Space)', database, <https://discosweb.esoc.esa.int/>, last accessed 15 March 2025
3. Spacetrack: 'Spacetrack webpage', database, <https://www.space-track.org/>, last accessed 15 March 2025
4. N. L. Johnson, P. H. Krisko, J.-C. Liou, P. D. Anz-Meador: 'NASA's New Breakup Model of Evolve 4.0', *Advances in Space Research*, Vol. 28., No. 9, pp. 1377-1384, 2001
5. W. Fucke, H. Sdunnus: 'Population Model of Small Size Space Debris – Final report', 1993
6. D. McKnight, R. Maher, L. Nagl: 'Refined Algorithms for Structural Breakup due to Hypervelocity Impact', *International Journal of Impact Engineering*, Vol. 17, pp. 547-558, 1995
7. M. E. Sorge: 'Satellite Fragmentation Modeling with IMPACT', *AIAA/AAS Astrodynamics Specialist Conference and Exhibit*, Honolulu, Hawaii, 2008
8. R. L. Andrişan, A. G. Ioniţă, R. D. González, et al.: 'Fragmentation Event Model and Assessment Tool (FREMAT) Supporting On-Orbit Fragmentation Analysis', *Proc. of the 7<sup>th</sup> European Conference on Space Debris*, Darmstadt, Germany, 2017
9. A. Francesconi, C. Giacomuzzo, L. Olivieri, et al.: 'CST: A new semi-empirical tool for simulating spacecraft collisions in orbit', *Acta Astronautica*, Vol. 160, pp. 195-205, 2019
10. M. Romano, A. Muciaccia, M. Trisolini, et al.: 'PUZZLE Software for the Characterisation of in-orbit Fragmentations', *Proc. of the 8<sup>th</sup> European Conf. on Space Debris*, Darmstadt, Germany, 2021

11. T. Yao, Z. Yang, Y. Luo, et al.: 'Generation of initial debris cloud distributions for breakup events based on CARDC-SBM', *Acta Astronautica*, Vol. 219, pp. 580-591, 2024
12. A. Horstmann: 'Final Report – Enhancement of S/C Fragmentation and Environment Evolution Models', <https://sdup.esoc.esa.int/master/downloads>, 2020
13. M. Pierzyna: 'Characterisation of on-orbit fragmentation events based on TLE data', Master's thesis, Technische Universität Braunschweig, 2022
14. NASA (National Aeronautics and Space Administration): 'Orbital Debris – Quarterly News', report, Vol. 27, Issue 1, 2023
15. D. L. Mains, M. E. Sorge, V. H. Cabrera: 'Techniques for quick-response representations of fragmentation events', *2nd International Orbital Debris Conference*, Sugar Land, Texas, 2023
16. M. F. Montaruli, S. Bonaccorsi, A. Muciaccia, et al: 'Assessment of the CZ-6A R/B and the H-2A DEB fragmentation events', *Aerospace Europe Conference*, Lausanne, Switzerland, 2023
17. NASA: 'Orbital Debris – Quarterly News', report, Vol. 28, Issue 4, 2024
18. B. Rhodes: 'SGP4 2.20', Python package, <https://pypi.org/project/sgp4/>, 2021
19. CelesTrak: 'EOP and Space Weather Data', database, <https://celestak.org/SpaceData/>, last accessed 20 February 2025